UC Berkeley
UC Berkeley Previously Published Works

Title

Multiphoton and Harmonic Imaging of Microarchitected Materials

Permalink

https://escholarship.org/uc/item/9tj251bw

Journal

ACS Applied Materials & Interfaces, 17(2)

ISSN

1944-8244

Authors

Blankenship, Brian W

Pan, Daisong

Kyriakou, Eudokia

et al.

Publication Date

2025-01-15

DOI

10.1021/acsami.4c16509

Peer reviewed

Research Article

Multiphoton and Harmonic Imaging of Microarchitected Materials

Brian W. Blankenship,[#] Daisong Pan,[#] Eudokia Kyriakou, Gordon Zyla, Timon Meier, Sophia Arvin, Nathan Seymour, Natalia De La Torre, Maria Farsari, Na Ji, and Costas P. Grigoropoulos*
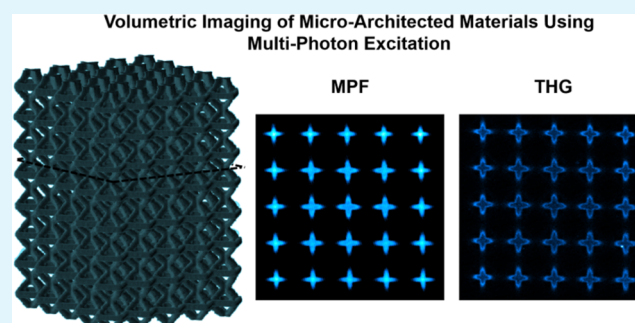
Read Online

ACCESS | Metrics & More | Article Recommendations | Supporting Information

ABSTRACT: Microadditive manufacturing has revolutionized the production of complex, nano- to microscale components across various fields. This work investigates two-photon (2P) and three-photon (3P) fluorescence imaging, as well as third-harmonic generation (THG) microscopy, to examine periodic micro-architected lattice structures fabricated using multiphoton lithography (MPL). By immersing the structures in refractive index matching fluids, we demonstrate high-fidelity 3D reconstructions of both fluorescent structures using 2P and 3P microscopy as well as low-fluorescence structures using THG microscopy. These results show that multiphoton fluorescence (MPF) imaging offers reduced signal decay with respect to depth compared to single-photon techniques in the examined structures. We further demonstrate the ability to nondestructively identify intentional internal modifications of the structure that are not immediately visible with scanning electron microscope (SEM) images and compression-induced fractures, highlighting the potential of these techniques for quality control and defect detection in microadditively manufactured components.

Volumetric Imaging of Micro-Architected Materials Using Multi-Photon Excitation — MPF — THG

KEYWORDS: microarchitected materials, two-photon polymerization, additive manufacturing, multiphoton imaging, polymers, defects

■ INTRODUCTION

Microadditive manufacturing has opened up entirely new fabrication capabilities, enabling the production of polymers,[1] ceramics,[2−5] and metallic[6,7] components with incredible geometric complexity and nano- to microscale feature sizes.[8−10] These components are finding increasing applications in diverse fields spanning optics,[11,12] quantum information science,[13,14] tissue engineering,[15,16] microfluidics,[17,18] and metamaterials.[19−21] Multiphoton lithography (MPL) has emerged as preeminent fabrication technique for these applications given its exceptional resolution (minimum resolutions below 100 nm) and rapid volumetric print rates exceeding 10^6 $\mu m^3/s$ at ∼1 μm voxel size.[22] Commercially available systems now routinely fabricate millimeter-sized parts with submicrometer precision, while ongoing advancements in materials science and processing technologies promise to push these boundaries to further extremes.[23]

The imperative for advanced optical imaging techniques to examine microadditively manufactured prints is 2-fold. First, as these components become more complex and permeate into an increasing number of applications there becomes a greater need to control their quality and inspect them. However, the diminutive scale and often intricate internal architectures of these components present challenges to conventional metrology techniques. Scanning electron microscopy (SEM) and laser profilometry offer high-resolution surface imaging but are inherently limited in their capacity to probe subsurface

structures. Moreover, SEM often requires the application of conductive surface coatings that can modify the optical properties of these materials. X-ray computerized tomography (CT), though capable of providing three-dimensional internal structure analysis, requires specialized radiation sources to achieve the necessary resolution to identify critical defects at nano- and microscales. Optical diffraction tomography has also emerged as a potential candidate for imaging structures fabricated by MPL,[24] but this technique may be limited by the depth of imaging and allowable complexity of structure.

Furthermore, microadditively manufactured structures are increasingly utilized as scaffolds for catalytic materials,[25] sensing particles,[13] as well as cellular cultures.[15] These systems offer a wealth of information that can be captured to understand the local environmental conditions and monitor cellular interactions. In these contexts, optical imaging leverages compatibility with various visible-light based chemical spectroscopies and engineered cell lines as well
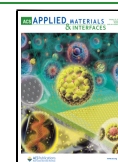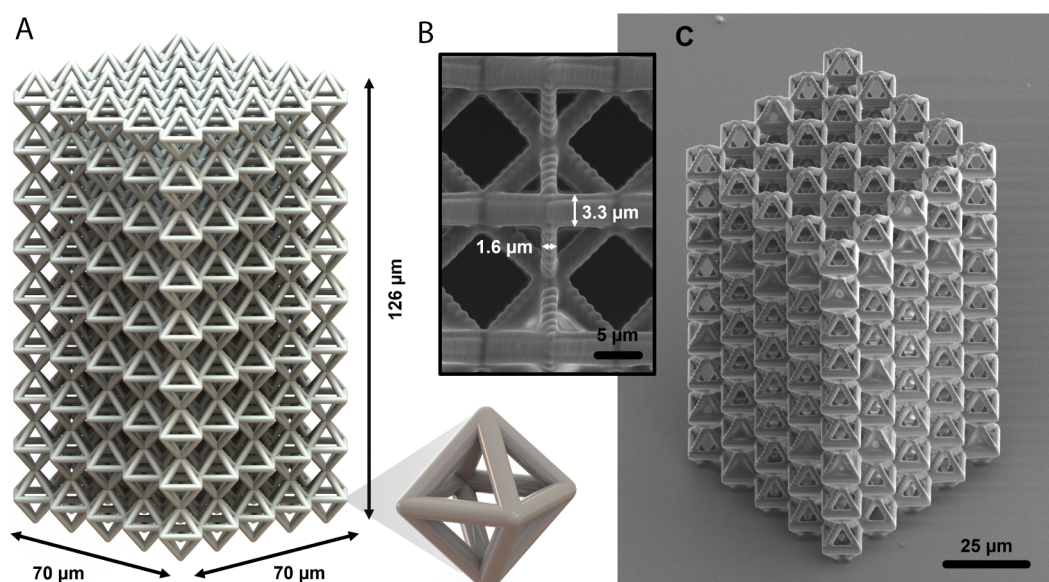
Figure 1. Structure design and fabrication. (A) CAD rendering of the 5 × 5 × 9 lattice composed of 14 μm × 14 μm × 14 μm periodic "diamond" unit cells used for benchmarking in this study. (B) Closeup of the unit cells of the structure as fabricated by MPL depicting beam members with lateral dimensions of 1.6 μm and axial dimensions of 3.3 μm. (C) An orthogonal view of the template structure as fabricated.

utilizing nonionizing radiation that could enable *in situ* imaging of cells within microarchitected tissue scaffolds.

The utility of single-photon optically sectioned microscopy techniques using refractive index (RI) matching fluids has been demonstrated for imaging microstructures fabricated with MPL with resolution commensurate with print capabilities.[26,27] These approaches are able to resolve cracks, defects, and applied microdeformations while permitting high-fidelity 3D reconstructions of their geometries.[26] In this work, we aim to expand on these techniques by employing multiphoton and harmonic imaging methods and exploring their strengths, limitations, and potential for enabling new applications in the nondestructive characterization of microadditively manufactured components. Moreover, these techniques can be conceivably integrated into a singular setup with both fabrication and imaging capabilities.

We investigate two-photon (2P) and three-photon (3P) fluorescence imaging of periodic microarchitected lattice structures, which serve as a benchmark for extreme cases of complex internal featuring in microadditively manufactured components. Both nonlinear imaging techniques demonstrated reduced scattering, indicating better depth penetration compared to our previously demonstrated single-photon technique. Meanwhile, by harnessing the capability of third-harmonic generation microscopy in probing interfaces where local changes in refractive index occur, we image low-fluorescence polymeric materials using this technique. Ultimately, we demonstrate the ability to create high-fidelity reconstructions of both fluorescent and suppressed-fluorescence structures with several different multiphoton imaging techniques.

RESULTS AND DISCUSSION

Lattice Structure Geometry and Fabrication. Several sets of 70 μm × 70 μm × 126 μm lattice structures composed of periodic diamond unit cells were fabricated using a custom MPL setup, employing the design shown in Figure 1A. This design was chosen to represent a complex, internally structured

component whose interior is ordinarily challenging to image using SEM or widefield optical microscopy, while providing periodic structures that enable easy benchmarking with depth. The height of the structure was selected to be smaller than the working distance of common oil-immersion lenses. Two types of resins were separately printed onto glass coverslips, both variants of a SZ2080, but made with different photoinitiators to modulate the fluorescence. One variant utilizes PI 4,4′-bis(diethylamino)benzophenone to produce highly fluorescent structures[28] and the other utilizes Sudan Black B to produce structures with low fluorescence.[29] Details on the resin preparation and processing parameters are provided in the Materials and Methods section. SEM images of one of the printed structures are shown in Figure 1B,C revealing the high-fidelity reproduction of the designed lattice via MPL. The axial and lateral dimensions of the printed beam members were measured to be on average 3.3 and 1.6 μm, respectively for structures of both resin compositions.

Multiphoton Fluorescence Imaging. 2P and 3P fluorescence imaging, hereafter referred to as multiphoton fluorescence imaging (MPF), were employed to visualize the internal structure of microadditively manufactured fluorescent SZ2080 samples in addition to the confocal single-photon fluorescence imaging. MPF confines fluorophore excitation to the focal plane requiring the simultaneous absorption of multiple photons of near-infrared wavelengths to excite the fluorophore.[30] This nonlinear absorption process reduces out-of-focus excitation and enables optical sectioning without the need for a pinhole detection aperture.

The feature sizes of the lattice structures used in this study are commensurate with the wavelength of the excitation source, with a feature size-to-wavelength ratio ranging from approximately 0.3 to 1 for the excitation wavelengths used (405–1300 nm). Consequently, strong scattering is expected when imaging the structure in low-RI medium such as air.[31] Indeed, when the samples are imaged in air, the signal from the lattice structure cannot be resolved further than a single layer into the structure (see Figure S1).
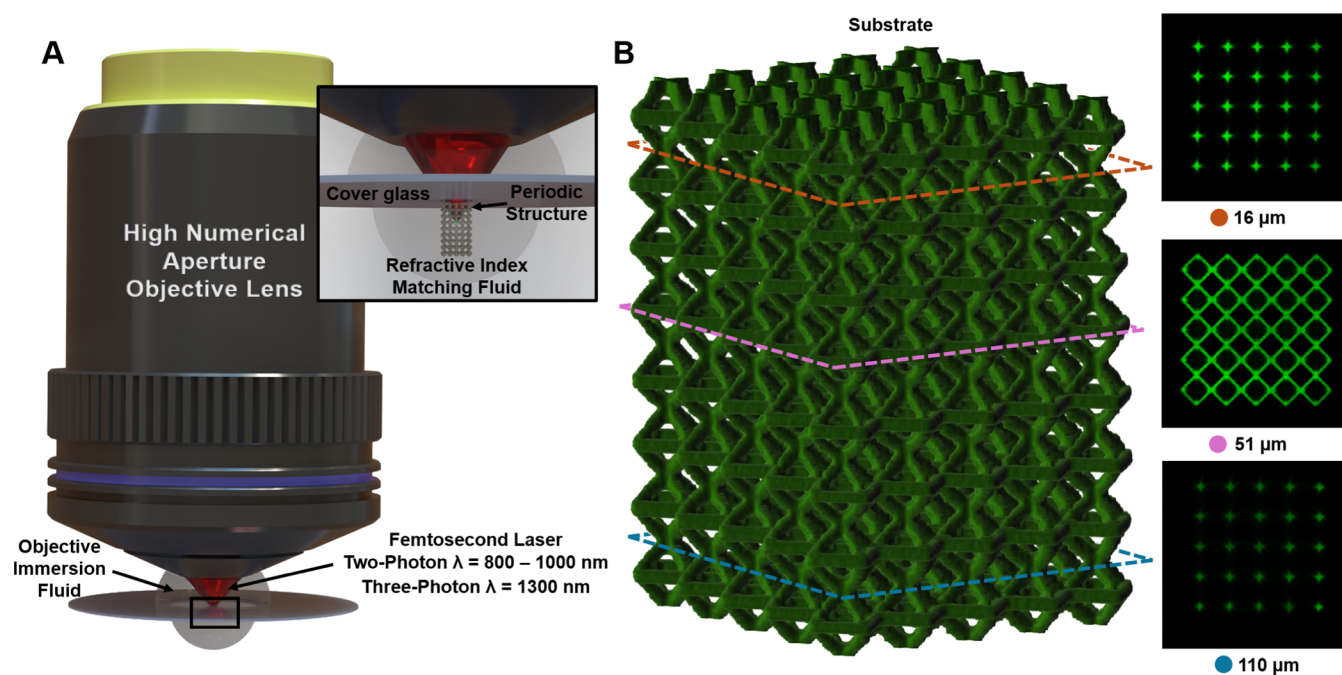
Figure 2. Multiphoton imaging setup and renderings. (A) The optical configuration for imaging microarchitected structures. On one side, the printed structure is enveloped in a RI matching fluid that roughly matches the RI of the polymer. On the other side, the lens is immersed in immersion oil or water based on the specifications of the objective lens. (B) A 3D rendering of the first 8 layers of the structure shown in Figure 1A along with corresponding two-photon fluorescence images of slices used to construct the rendering which are labeled by their successive depth into the structure from the substrate.

To mitigate strong scattering and enable deeper imaging, the structures were immersed in an RI-matching oil (RI = 1.518).[32] Figure 2A illustrates this general imaging setup. This immersion approach facilitates the reconstruction of three-dimensional renderings of both the lattice structure as well as nonporous geometries. Air—oil interfaces sometimes formed above the layer furthest from the glass substrate, resulting in inconsistent imaging quality through the last layer of the structure. Consequently, we limit our analysis to the first eight layers of the structures (see Figure S2). Additionally, the longer excitation wavelengths utilized in 3P, and to a lesser extent 2P, are expected to incurt reduced scattering using these techniques relative to a single photon (1P) imaging counterpart, as scattering is wavelength dependent.

We employed a commercial two-photon microscope (see Materials and Methods) to capture fluorescence images sampled at 500 nm intervals along the z axis. These images were used to construct the rendering displayed in Figure 2B. In individual slices there is clear contrast from the polymerized sections relative to the RI matching oil that enables a clear visualization of the structure's internal architecture. The images are then binarized using an Otsu thresholding algorithm to construct the lattice in popular 3D modeling formats. 3D models of the structure can likewise be recreated using 1P and 3P fluorescence imaging.

The fluorescence of the SZ2080 samples primarily originates from the excitation of residual photoinitiator, 4,4′-Bis-(diethylamino)benzophenone.[27] Many other photoinitiators commonly used in multiphoton lithography, including those in commercial resins, are also fluorescent.[29] The 2P fluorescence spectrum of 4,4′-Bis(diethylamino)benzophenone, as incorporated into the structures and measured using 780 nm, 100 fs excitation, exhibits a broad, multipeaked emission from 500 to 700 nm with maximum emission around 540 nm (Figure S3).

For multiphoton excitation the time averaged photon flux from an excited fluorophore scales according to the relationship:[33]

$$F^{(n)}(t) \propto \sigma_n I(t)^n$$

Where $F^{(n)}(t)$ is the time photon flux from n^{th} order excitation, $I(t)$ intensity, and σ_n is the n-photon absorption cross section.

To confirm that the signal came from the two-photon excitation, we imaged identical layers of the sample using a range of excitation wavelengths while varying the laser power. The fluorescence signal, expected to follow a quadratic dependence on time-averaged power ($\propto P^2$), was analyzed for excitation at 800, 900, and 1000 nm. Figure 3A presents log—log plots of fluorescence intensity versus time-averaged power sampled at consistent locations on the structure. In an ideal case, the slope of a log—log plot of fluorescence intensity vs excitation power relates to the nth order excitation experienced by a fluorophore. The slopes derived from these plots are calculated to be $n = 1.86 \pm 0.13$, $n = 1.91 \pm 0.06$, and $n = 1.96 \pm 0.16$, respectively, affirming the two-photon excitation process. These measurements also indicate that 800 nm excitation yields the highest excitation efficiency among the tested wavelengths, although imaging remains viable at 900 and 1000 nm. This finding highlights the potential for 3D diagnostic imaging of samples during fabrication via 2P excitation at higher wavelengths that do not readily induce resin polymerization, assuming sufficient fluorescence contrast between polymerized and nonpolymerized resin. Such a behavior can be anticipated intrinsically due to the local environment change upon polymerization.

An alternative microscope setup (see Materials and Methods) was used to examine the 3P fluorescence and third harmonic generation (THG) signal from the sample at
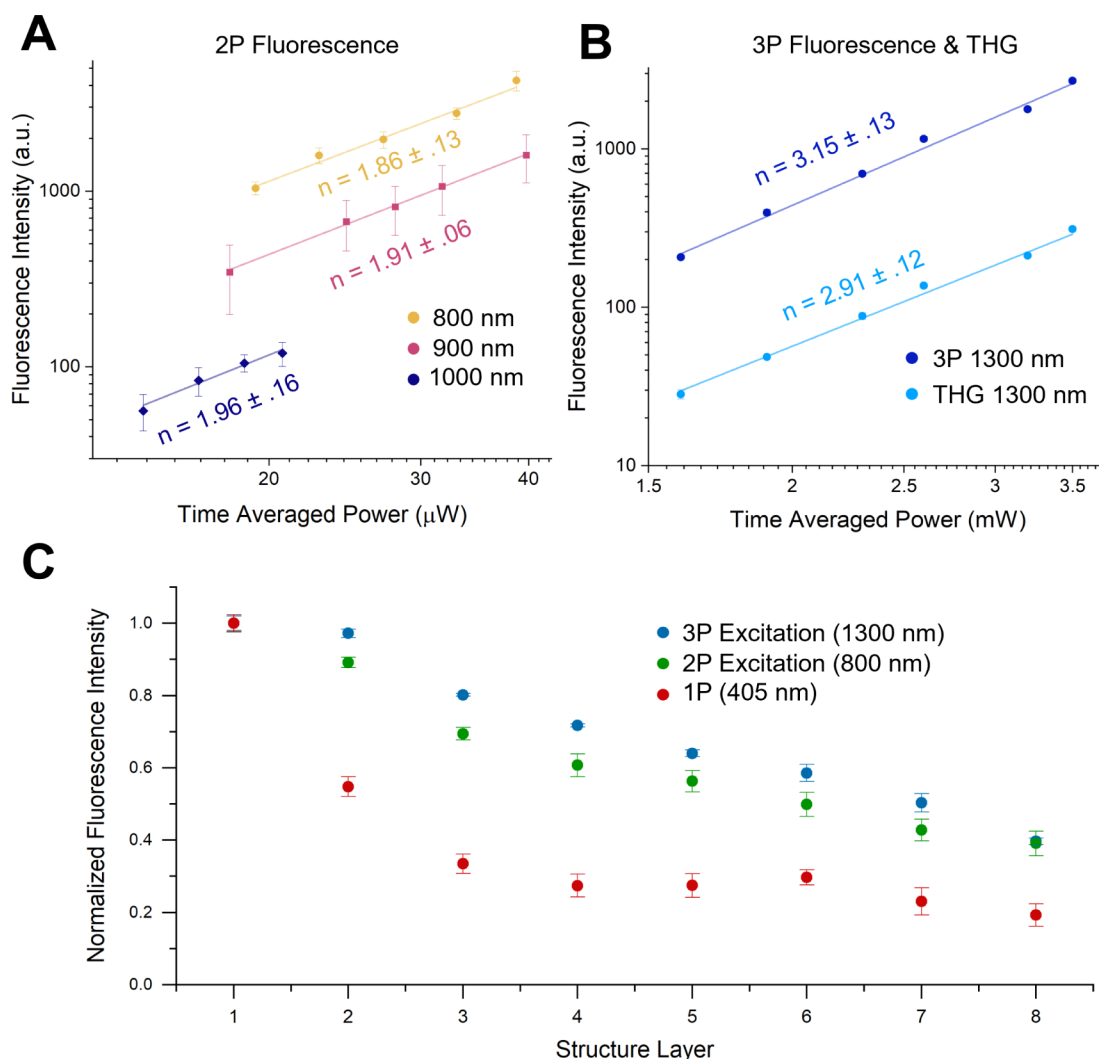
Figure 3. Fluorescence intensity vs power and layer depth. (A) Fluorescence intensity vs time averaged power for 800, 900, and 1000 nm excitation. The log−log slope of excitation vs power was measured to be 1.86 ± 0.13, 1.91 ± 0.06, and 1.96 ± 0.16, respectively, which is suggestive of 2P excitation. Of the measured wavelengths, 800 nm was found to have the highest excitation efficiency. (B) Similar measurements were taken for 3P excitation at 1300 nm. In this case, the log−log slope of optical signal vs power was measured to be 3.15 ± 0.13 for the 3P channel and 2.91 ± 0.12 for the THG channel. (C) Normalized fluorescence intensity versus the measured layer into the structure. Collected fluorescence signal from multiphoton excitation process appear to decay less rapidly than via 1P excitation.

1300 nm excitation. As in the 2P fluorescence imaging runs, it is possible to produce high-quality optically sectioned slices of each layer of the lattice structure. In this case, the corresponding optical signals were expected to follow a cubic dependence on time-averaged power $(\propto P^3)$.[3] Figure 3B presents log−log plots of optical signal intensity versus time-averaged power, sampled at identical locations across the images, yielding a slope of $n = 3.15 \pm 0.13$ for the 3P fluorescence channel, and a slope of $n = 2.91 \pm 0.12$ for the THG channel.

Signal Decay Across Depth. Fluorescence signal decay for single (405 nm), 2P (800 nm), and 3P (1300 nm) excitation into the first 8 layers of the sample is measured at consistent locations across different layers. The normalized fluorescence intensity profiles relative to the first-layer fluorescence are presented in Figure 3C. These profiles reveal a markedly reduced signal decay for both two-photon and three-photon imaging modalities compared to single-photon excitation. The disparity in signal decay is most pronounced at the second layer, where the fluorescence intensity for single-

photon excitation decreases to 54.8% ± 2.7% of its initial value. In contrast, the two-photon and three-photon images retain 89.1% ± 1.4% and 97.2% ± 1.2% of the initial signal intensity, respectively. MPF consistently outperforms single-photon imaging at every subsequent layer; ultimately, the single-photon signal intensity diminishes to just 19.3% ± 3.1% at the eight layer whereas two-photon and three-photon imaging retain higher intensities of 39.1% ± 3.3% and 39.7% ± 0.9%, respectively. The acquired signal depicts a roughly exponential decay, although a modest upward trend at layers 5 and 6 is observed in the single photon image set. These results highlight the advantage of reduced scattering in multiphoton techniques due to their longer excitation wavelengths.

Third Harmonic Generation Microscopy. THG microscopy is a complementary approach to MPF that offers unique advantages for characterizing complex microadditively manufactured structures, particularly those designed to have low autofluorescence such as in optical components.[34] THG microscopy relies on a fundamentally different contrast mechanism compared to fluorescence-based techniques. The
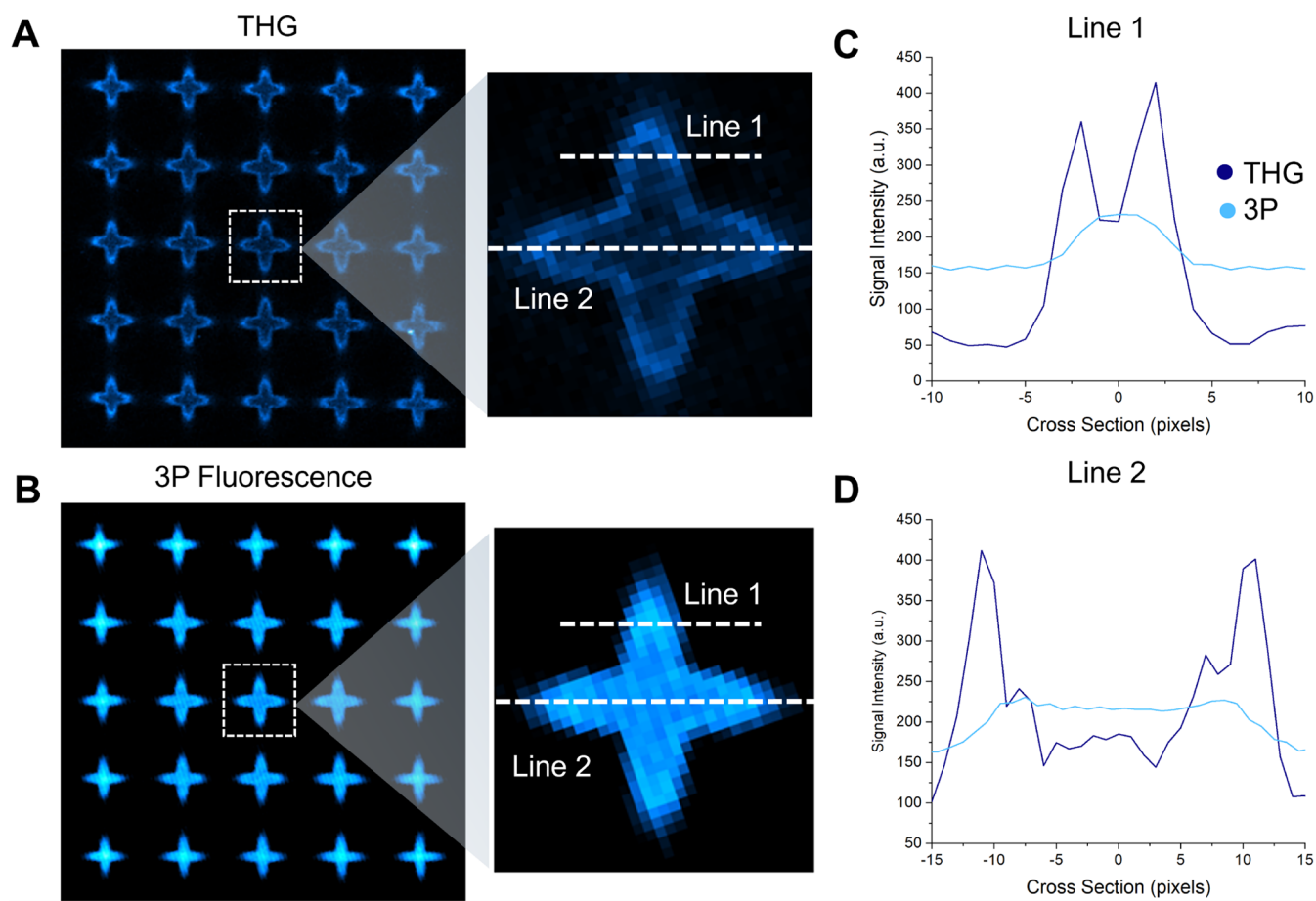
Figure 4. Comparison of THG to 3P fluorescence images. (A) THG cross section compared to (B) corresponding 3P fluorescence cross sections of the same slice. (C) Intensity profile of the two techniques from the central element in A and B are contrasted for the top profile (line 1) (D) and the central profile of the beam element (line 2).

third-harmonic signal is generated through a coherent, nonlinear optical process that upconverts three near-infrared photons into one visible wavelength photon with one-third the excitation wavelength. This signal stems from the third-order nonlinear susceptibility tensor, $\chi^{(3)}$. Under the tight focusing-condition formed by a high numerical aperture objective, local optical heterogeneities within the excitation beam focal zone generate contrast, thus making THG a sensitive probe for interfaces and inhomogeneities within samples (see Figure S2).[34−36] For complex microadditively manufactured components such as gradient refractive index optics, this attribute offers opportunities for high-contrast, label-free imaging of internal architectures and susceptibility variations.[37−39] Moreover, universal presence of nonvanishing third order susceptibility in materials means that THG microscopy can be applied to a wide range of samples, including those with low or suppressed fluorescence.[29,40]

Prior investigations have demonstrated the efficacy of using THG in imaging less complex, 2.5D structures fabricated via MPL both in air using resists with low fluorescence contrasts,[41] as well as the examination of polymerized material within undeveloped photoresists.[42] Herein we expand upon these capabilities to nondestructively examine the microarchitected lattice structure shown in Figure 1. Using the same optical setup as three-photon microscopy with an additional detection channel at a different wavelength, we investigate THG imaging of both the high-fluorescence and low-fluorescence photo-

polymers, demonstrating the technique's capacity to generate contrast from minimal RI interface differentials, despite its immersion in a medium with a closely matched RI.

Figure 4 compares images of a section of the micro-architected structure constructed from the low-fluorescence photopolymer taken with both THG (Figure 4A) and 3P fluorescence (Figure 4B). Intensity profiles of the central lattice element are shown in Figure 4C,D. Despite having a reduced fluorescence, multiphoton fluorescence is still generated in the Sudan B samples likely via excitation of ZrO_2 nanoparticles formed in the resin.[40] In contrast to the 3P images of lateral cross sections, wherein intensity is strongest toward the center of the beam, the THG image shows highest contrast at the interface between the polymer and the index matching oil, where the sharpest susceptibility mismatch happens within both the lateral and axial extent of the focus. Nonetheless, contrast remains above background in the center of the printed beam members, which is likely because the axial extent of the excitation focus still partially covers the material-RI fluid interface. Although it may be possible to heighten THG contrast at the material-RI fluid interface by using fluids with larger susceptibility mismatch, this likely comes at a trade-off with achievable imaging depth. Signal strength is likewise limited by exposure dose to the sample. In these experiments, it was found that the RI fluid would consistently begin to generate microbubbles using time averaged intensities exceeding 3.6 mW with a 204.8 × 204.8 μm^2 FOV.
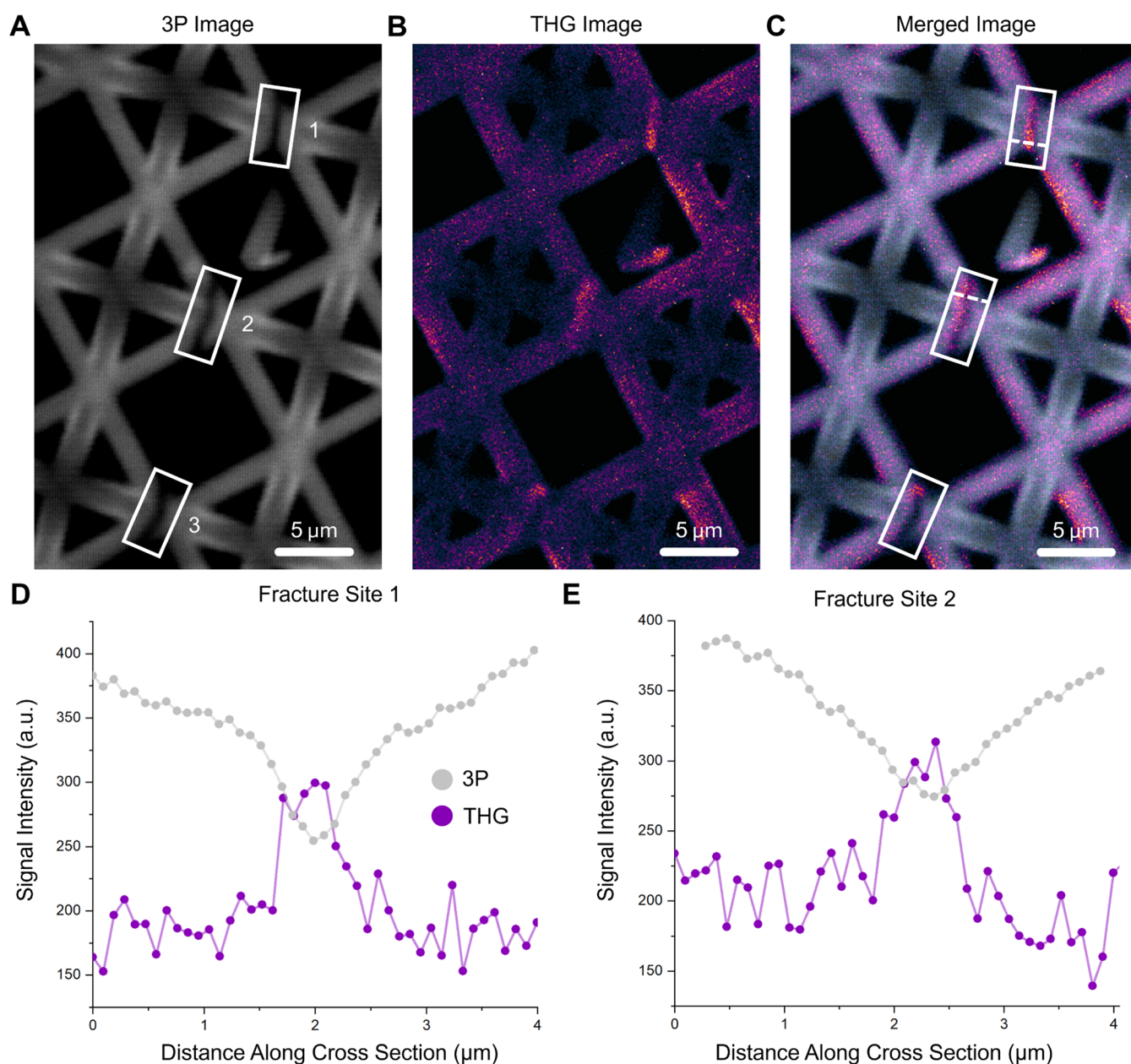
Figure 5. 3P and THG images of fracture beam members. (A) 3P image of a cross section with three cracked beam members (B) compared to the corresponding THG image measured at the slice position. (C) The merged image shows that THG contrast aligns with the location of cracks (D) 3P and THG signal intensity measured across the highlighted cross sections for fracture site #1 and (E) fracture site #2, where THG signal increases at these locations and THG signal decreases.

Defect Detection. Additively manufactured microarchitectures pose unique challenges for non-destructively identifying and characterizing defects that arise from either manufacturing processes or damage. The optical reconstruction techniques described herein address this challenge, enabling detailed inspection across a wide variety of constituent materials. These capabilities are indispensable for quality control, performance prediction, and failure analysis of microarchitected structures.

For example, we subjected several lattice structures to compressive loads until fracture. Figure 5A showcases 3P images of a cross-section featuring three distinct cracks, while Figure 5B displays the corresponding THG of the same region. The merged dual-color images in Figure 5C depict enhanced signal contrast at the crack locations, even for cracks where the

spacing between severed beam members at sites 1 and 2 is just ~1 μm across.

Figure 5D,E illustrates signal intensity profiles of 3P and THG along the highlighted cross sections for fracture sites 1 and 2. The fractured regions in the 3P images exhibit reduced fluorescence signal compared to the intact sections of the beam members. Conversely, the THG images show increased signal intensity at these locations. This contrast enhancement in the THG images arises from susceptibility mismatches at the crack sites, aligned with the prediction made based on the THG contrast mechanisms which highlights cracks with lateral and/ or axial dimension smaller than the focal size.

As another demonstration we fabricated a series of structures with intentional modifications: additional beam members spelling "LTL" (denoting Laser Thermal Laboratory) were
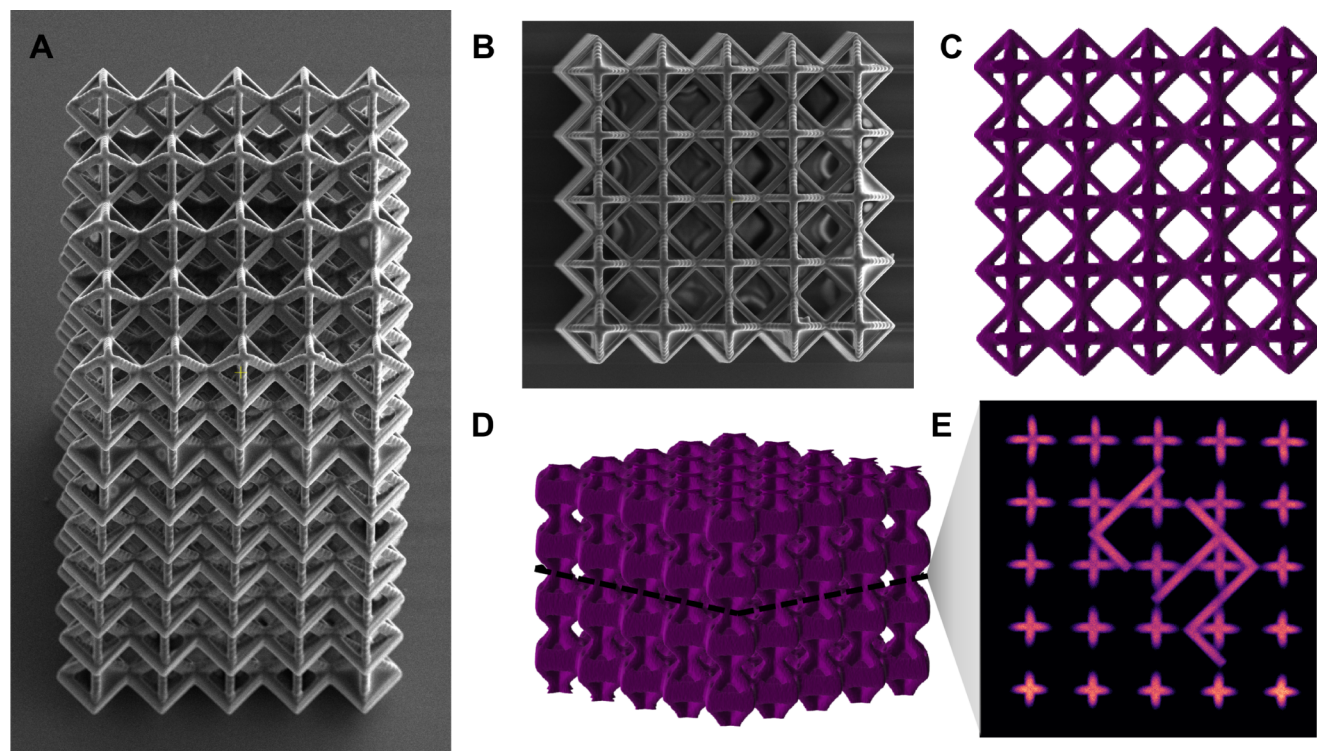
Figure 6. Nondestructive imaging of internal defects. (A) SEM images of a structure with extra beam members incorporated into the 4th layer of the structure. (B) Top-view SEM images where the extra beam members are not immediately visible. (C) Corresponding top down and (D) orthogonal view of the middle layers of the structure. (E) Hidden beams, spelling out LTL, are apparent within optically sectioned images taken via 2P microscopy images.

incorporated into the fourth layer of the lattice. This experiment tests the detection of internal structural anomalies that might arise from manufacturing defects or intentional design features. Hidden beam members inside the lattice structure are obscured from view within SEM images taken from various angles (Figure 6 A,B). In contrast, three-dimensional renderings constructed from stacked 2P image slices (Figure 6C,D, showing top-down and orthogonal views) reveal the hidden beam members (Figure 6E).

These demonstrations underscore the efficacy of multiphoton imaging techniques in nondestructively identifying and characterizing internal structural anomalies of both fluorescent and low-fluorescence materials. The ability to detect such features is crucial for quality control in advanced manufacturing processes, where internal defects or modifications can significantly impact the mechanical and functional properties of the final structure.[43,44]

CONCLUSION

This study demonstrates the efficacy of multiphoton imaging techniques for nondestructive characterization of complex microadditively manufactured structures. By employing a range of multiphoton imaging modalities, including 2P fluorescence, 3P fluorescence, and THG microscopy, we have demonstrated the capacity to generate high-fidelity 3D reconstructions of intricate internal architectures that are challenging to image with conventional techniques such as SEM.

These investigations reveal that multiphoton fluorescence imaging offers enhanced depth penetration compared to single-photon techniques within the lattice geometry that is examined. This benefit facilitates clearer visualization of deeper structural layers and becomes increasingly important as higher-

throughput multiphoton lithography enables the fabrication of larger and more complex architectures. Notably, single-photon signals decay sharply at greater depths following the trend shown in Figure 3C. While increasing excitation power can help compensate for signal decay, strong scattering ultimately limits 1P imaging depth by constraining its signal-to-noise and signal-to-background ratios (SNR and SBR), leading to a practically unmeasurable signal at greater depths. By contrast, 2P and 3P imaging methods are intrinsically less affected by scattering, enabling robust, high-fidelity imaging at greater depths into these structures.

Furthermore, we have shown that THG microscopy serves as a complementary, label-free imaging modality that is effective for examining structures with low autofluorescence and for detecting fractures within these materials.

The potential applications of multiphoton and harmonic imaging techniques extend far beyond the scope of this study. Future research could explore their utility in examining polymers fabricated without photoinitiators[45] as well as nonpolymeric materials such as glass,[46] calcinated,[5] or other inorganic materials,[47] opening new avenues for characterization across a broader range of micromanufactured components.[46] Additionally, these methods show promise for *in situ* monitoring of multiphoton lithography processes, potentially enabling real-time quality control during fabrication. The integration of high-speed, kilohertz multiphoton imaging systems could further expand capabilities, potentially allowing near-real-time imaging of dynamic mechanical loading events in these structures.[48] Such advancements would significantly enhance our understanding of material behavior at the microscale and improve the design and fabrication of complex microarchitected materials.

■ MATERIALS AND METHODS

Resin. SZ2080, a hybrid organic−inorganic photoresist enabling high-resolution 3D printing with minimal shrinkage,[49] was used as a photosensitive material to fabricate structures via MPL. The resist comprises Methacryloxypropyl trimethoxysilane (MAPTMS, 99%, Sigma-Aldrich) and methacrylic acid (MAA) as organic photo-polymerizable monomers, while zirconium n-propoxide (ZPO, 70%, Sigma-Aldrich) and the alkoxysilane groups of MAPTMS serve as the inorganic network. It was synthesized in-house by a sol−gel process. First, MAPTMS was hydrolyzed using an HCl solution (0.1 M) at a ratio of 1:0.1. Then, ZPO was stabilized by MAA at a molar ratio of 1:1, followed by stirring for 20 min. Afterward, the ZPO was slowly added to the hydrolyzed MAPTMS at a 2:8 molar ratio.

For the fabrication of the structures, SZ2080 photoresists were prepared with two different photoinitiators. While the PI 4,4′-bis(diethylamino)benzophenone (Michler's ketone, Sigma-Aldrich) enabled the production of high-fluorescent structures[28] and Sudan Black B (SBB; Sigma-Aldrich) enabled the production of structures with low fluorescence.[29]

Following the final synthesis step described above, 1% of Michler's ketone with respect to the monomers of SZ2080 was directly incorporated inside the material. In contrast, SBB was first diluted with isopropanol at a concentration of 1% w/v. Then, one tenth of this solution was added to the resist, resulting in a 0.3% concentration of SBB relative to the monomers of SZ2080. Each PI was stirred into SZ2080 for 15 min. Afterward, the photoresists were filtered using a 0.22 μm pore size syringe filter and subjected to a 1-h vacuum treatment to enhance viscosity. Subsequently, the samples were placed in a vacuum for 7 days to ensure the complete evaporation of any remaining solvent.

Fabrication. MPL was conducted using an ultrafast laser system (FemtoFiber ultra 780, Toptica Photonics AG, Germany). The laser system emits laser radiation with a central wavelength of 780 nm, a pulse duration of 150 fs, and a repetition rate of 80 MHz. The fabrication process was done in a layer-by-layer manner. Specifically, a galvo scanner and an acoustic optical modulator were employed to produce each layer of the structure, while the sample was shifted along its vertical axis using a linear stage after each layer was completed. Another two linear stages enabled the production of multiple structures on one coverslip. An overview of the optical setup, including detailed information on the components can be found in Zyla et al.[50] This way, structures were fabricated using microscope objective (40×/NA 1.4, oil-immersive, Plan-Apo, Zeiss, Germany) and a galvo scanner speed of 20 mm/s. The average laser power for the fabrication of high- and low-fluorescent structures was set to 8.5 mW and 12 mW, respectively. The values were measured at the entrance pupil of the microscope objective. The hatching and slicing parameters were set to 0.2 and 0.4 μm, respectively. The hatching pattern featured lines oriented in one direction, which were rotated by 90° for each subsequent layer. After MPL, the samples were developed in 4-methyl-2-pentanone (Sigma-Aldrich, Germany) for 2 h, followed by a 10 min immersion in isopropanol for cleaning.

RI Matching Fluid. Olympus type F, low autofluorescence immersion oil, $n = 1.518$ (TH-MOIL-30) was used as a refractive index matching fluid.

Single-Photon Imaging. An Olympus Fluoview 3000 laser scanning microscope was used for single-photon imaging using an excitation wavelength of 405 nm and using a 405 nm long pass filter. Images were generated of the structure at a pixel resolution of 1024 × 1024- and 12-bit intensity resolution. A 60×, 1.35 NA oil dipping objective (Olympus) was used.

Two-Photon Imaging. 2P images were acquired using a Bruker 2P Plus multiphoton microscope. Excitation was provided by a Chameleon tunable wavelength laser, with an operating range of 680−1064 nm. Fluorescence emission from the sample was collected through a bandpass filter (525/70 nm) to multialkali PMTs to generate the final images. A 60×, 1.35 NA oil dipping objective (Olympus) was used. XY pixel sizes for the image in Figure 2 are roughly 180 nm.

Three-Photon Fluorescence and Third Harmonic Imaging. 3P fluorescence and THG imaging were performed on a custom-built microscopy system. The optical setup has been described in detail previously.[51] An optical parametric amplifier (Opera-F, Coherent) is pumped by a 40-W femtosecond laser (Monaco 1035-40-40, Coherent) to generate 1300 nm output at 1 MHz. The output beam is scanned with a pair of conjugated galvanometric scanning mirrors (6215H, Cambridge Technology) and relayed to the back-pupil plane of a high NA water-dipping objective (Olympus XLPLN25XWMP2, NA 1.05, 25×) using two pairs of scan lenses (SL50-3P and SL50-3P, SL50-3P and TTL200MP; Thorlabs). The correction collar was adjusted to match the thickness of the coverslip. A home-built single-prism compressor[52] is employed to compensate for the group delay dispersion (GDD) of the excitation beam path, achieving a pulse duration of ∼54 fs at the focal plane of the objective. The objective is mounted on a piezoelectric stage (p-725.4CD PIFOC, Physik Instrumente) for axial translation of the excitation focus. The fluorescence and THG signals are collected by the same objective, reflected by a dichroic mirror (FF665-Di02-25×36, Semrock). An additional dichroic mirror (Dm, FF458-Di02-25×36, Semrock) and two filters (FF03-525/50-25 for fluorescence, FF01-433/24-25 for THG; Semrock) are used to split and filter the 3PF and THG signals, which are then detected by two photomultiplier tubes (H10770PA-40, Hamamatsu).

Signal Intensity vs Applied Power Measurements. To account for rapid photobleaching of fluorescence in MPL-fabricated structures, signal vs applied power measurements were performed twice: first with increasing power, then again with decreasing power. This approach compensates for photobleaching effects.

SEM Imaging. Structures were sputter-coated using Au target, resulting in a 10 nm-thick film and imaged in a Scios 2 DualBeam SEM.

■ ASSOCIATED CONTENT

ⓢ Supporting Information

The Supporting Information is available free of charge at https://pubs.acs.org/doi/10.1021/acsami.4c16509.

> 3P images of lattice structures at different depths taken in air, cross sectional 3P and THG images, 2P fluorescence spectrum of SZ2080 resin, and 1P and 3P beam width measurements across depth (PDF)

■ AUTHOR INFORMATION

Corresponding Author

Costas P. Grigoropoulos − *Laser Thermal Laboratory, Department of Mechanical Engineering, University of California, Berkeley, California 94720, United States;* ⓞ orcid.org/0000-0002-8505-4037; Email: cgrigoro@berkeley.edu

Authors

Brian W. Blankenship − *Laser Thermal Laboratory, Department of Mechanical Engineering, University of California, Berkeley, California 94720, United States;* ⓞ orcid.org/0000-0003-4212-6835

Daisong Pan − *Department of Physics, University of California, Berkeley, California 94720, United States*

Eudokia Kyriakou − *Institute of Electronic Structure and Laser, Foundation for Research and Technology, GR-70013 Heraklion, Crete, Greece; Department of Materials Science and Technology, University of Crete, Heraklion GR-70013, Greece*

Gordon Zyla − *Institute of Electronic Structure and Laser, Foundation for Research and Technology, GR-70013 Heraklion, Crete, Greece;* ⓞ orcid.org/0000-0001-8202-1574

Timon Meier − *Laser Thermal Laboratory, Department of Mechanical Engineering, University of California, Berkeley, California 94720, United States;* ⊙ orcid.org/0009-0009-6572-680X

Sophia Arvin − *Laser Thermal Laboratory, Department of Mechanical Engineering, University of California, Berkeley, California 94720, United States;* ⊙ orcid.org/0009-0008-3525-9086

Nathan Seymour − *Laser Thermal Laboratory, Department of Mechanical Engineering, University of California, Berkeley, California 94720, United States*

Natalia De La Torre − *Laser Thermal Laboratory, Department of Mechanical Engineering, University of California, Berkeley, California 94720, United States*

Maria Farsari − *Institute of Electronic Structure and Laser, Foundation for Research and Technology, GR-70013 Heraklion, Crete, Greece*

Na Ji − *Department of Physics, University of California, Berkeley, California 94720, United States*

Complete contact information is available at:
https://pubs.acs.org/10.1021/acsami.4c16509

Author Contributions

#B.W.B. and D.P. contributed equally to this work.

Notes

The authors declare no competing financial interest.

■ REFERENCES

(1) Maruo, S.; Nakamura, O.; Kawata, S. Three-Dimensional Microfabrication with Two-Photon-Absorbed Photopolymerization. *Opt. Lett.* **1997**, *22* (2), 132−134.

(2) Ovsianikov, A.; Gaidukeviciute, A.; Chichkov, B.; Oubaha, M.; MacCraith, B. D.; Sakellari, I.; Giakoumaki, A.; Gray, D.; Vamvakaki, M.; Farsari, M.; Fotakis, C.; et al. Two-Photon Polymerization of Hybrid Sol-Gel Materials for Photonics Applications. *Laser Chem.* **2008**, *2008* (1), 493059.

(3) Jang, D.; Meza, L. R.; Greer, F.; Greer, J. R. Fabrication and Deformation of Three-Dimensional Hollow Ceramic Nanostructures. *Nat. Mater.* **2013**, *12* (10), 893−898.

(4) Meza, L. R.; Das, S.; Greer, J. R. Strong, Lightweight, and Recoverable Three-Dimensional Ceramic Nanolattices. *Science* **2014**, *345*, 1322.

(5) Balčas, G.; Malinauskas, M.; Farsari, M.; Juodkazis, S. Fabrication of Glass-Ceramic 3D Micro-Optics by Combining Laser Lithography and Calcination. *Adv. Funct. Mater.* **2023**, *33* (39), 2215230.

(6) Saccone, M. A.; Gallivan, R. A.; Narita, K.; Yee, D. W.; Greer, J. R. Additive Manufacturing of Micro-Architected Metals via Hydrogel Infusion. *Nature* **2022**, *612* (7941), 685−690.

(7) Zheng, X.; Smith, W.; Jackson, J.; Moran, B.; Cui, H.; Chen, D.; Ye, J.; Fang, N.; Rodriguez, N.; Weisgraber, T.; et al. Multiscale Metallic Metamaterials. *Nat. Mater.* **2016**, *15* (10), 1100−1106.

(8) Gross, A. J.; Bertoldi, K. Additive Manufacturing of Nanostructures That Are Delicate, Complex, and Smaller than Ever. *Small* **2019**, *15* (33), 1902370.

(9) Wollhofen, R.; Katzmann, J.; Hrelescu, C.; Jacak, J.; Klar, T. A. 120 Nm Resolution and 55 Nm Structure Size in STED-Lithography. *Opt. Express* **2013**, *21* (9), 10831−10840.

(10) Han, F.; Gu, S.; Klimas, A.; Zhao, N.; Zhao, Y.; Chen, S.-C. Three-Dimensional Nanofabrication via Ultrafast Laser Patterning and Kinetically Regulated Material Assembly. *Science* **2022**, *378* (6626), 1325−1331.

(11) Thiele, S.; Arzenbacher, K.; Gissibl, T.; Giessen, H.; Herkommer, A. M. 3D-Printed Eagle Eye: Compound Microlens System for Foveated Imaging. *Sci. Adv.* **2017**, *3* (2), No. e1602655.

(12) Kubec, A.; Zdora, M.-C.; Sanli, U. T.; Diaz, A.; Vila-Comamala, J.; David, C. An Achromatic X-Ray Lens. *Nat. Commun.* **2022**, *13* (1), 1305.

(13) Blankenship, B. W.; Jones, Z.; Zhao, N.; Singh, H.; Sarkar, A.; Li, R.; Suh, E.; Chen, A.; Grigoropoulos, C. P.; Ajoy, A. Complex Three-Dimensional Microscale Structures for Quantum Sensing Applications. *Nano Lett.* **2023**, *23* (20), 9272−9279.

(14) Xu, S.; Xia, X.; Yu, Q.; Khan, S.; Megidish, E.; You, B.; Hemmerling, B.; Jayich, A.; Biener, J.; Häffner, H.; 3D-Printed Micro Ion Trap Technology for Scalable Quantum Information Processing. *arXiv.org* .

(15) Flamourakis, G.; Spanos, I.; Vangelatos, Z.; Manganas, P.; Papadimitriou, L.; Grigoropoulos, C.; Ranella, A.; Farsari, M. Laser-Made 3D Auxetic Metamaterial Scaffolds for Tissue Engineering Applications. *Macromol. Mater. Eng.* **2020**, *305* (7), 2000238.

(16) Song, J.; Michas, C.; Chen, C. S.; White, A. E.; Grinstaff, M. W. From Simple to Architecturally Complex Hydrogel Scaffolds for Cell and Tissue Engineering Applications: Opportunities Presented by Two-Photon Polymerization. *Adv. Healthcare Mater.* **2020**, *9* (1), 1901217.

(17) McLennan, H. J.; Blanch, A. J.; Wallace, S. J.; Ritter, L. J.; Heinrich, S. L.; Gardner, D. K.; Dunning, K. R.; Gauvin, M. J.; Love, A. K.; Thompson, J. G. Nano-Liter Perfusion Microfluidic Device Made Entirely by Two-Photon Polymerization for Dynamic Cell Culture with Easy Cell Recovery. *Sci. Rep.* **2023**, *13* (1), 562.

(18) Vanderpoorten, O.; Peter, Q.; Challa, P. K.; Keyser, U. F.; Baumberg, J.; Kaminski, C. F.; Knowles, T. P. J. Scalable Integration of Nano-, and Microfluidics with Hybrid Two-Photon Lithography. *Microsyst. Nanoeng.* **2019**, *5* (1), 1−9.

(19) Meier, T.; Li, R.; Mavrikos, S.; Blankenship, B.; Vangelatos, Z.; Yildizdag, M. E.; Grigoropoulos, C. P. Obtaining Auxetic and Isotropic Metamaterials in Counterintuitive Design Spaces An Automated Optimization Approach And Experimental Characterization. *Npj Comput. Mater.* **2024**, *10* (1), 1−12.

(20) Kai, Y.; Dhulipala, S.; Sun, R.; Lem, J.; DeLima, W.; Pezeril, T.; Portela, C. M. Dynamic Diagnosis of Metamaterials through Laser-Induced Vibrational Signatures. *Nature* **2023**, *623* (7987), 514−521.

(21) Barchiesi, E.; Mavrikos, S.; Giorgio, I.; Grigoropoulos, C.; Farsari, M.; Dell'isola, F.; Zyla, G. Complex Mechanical Properties of 3D Micro-Metric Pantographic Metamaterials Fabricated by Two-Photon Polymerization. *Continuum Mech. Thermodyn.* **2024**, *36*, 1755.

(22) Somers, P.; Münchinger, A.; Maruo, S.; Moser, C.; Xu, X.; Wegener, M. The Physics of 3D Printing with Light. *Nat. Rev. Phys.* **2024**, *6* (2), 99−113.

(23) Zyla, G.; Farsari, M. Frontiers of Laser-Based 3D Printing: A Perspective on Multi-Photon Lithography. *Laser Photonics Rev.* **2024**, *18* (7), 2301312.

(24) He, Y.; Shao, Q.; Chen, S.-C.; Zhou, R. Characterization of Two-Photon Photopolymerization Fabrication Using High-Speed Optical Diffraction Tomography. *Addit. Manuf.* **2022**, *60*, 103293.

(25) Giakoumaki, A. N.; Kenanakis, G.; Klini, A.; Androulidaki, M.; Viskadourakis, Z.; Farsari, M.; Selimis, A. 3D Micro-Structured Arrays of ZnO Nanorods. *Sci. Rep.* **2017**, *7* (1), 2100.

(26) Blankenship, B. W.; Meier, T.; Zhao, N.; Mavrikos, S.; Arvin, S.; De La Torre, N.; Hsu, B.; Seymour, N.; Grigoropoulos, C. P. Three-Dimensional Optical Imaging of Internal Deformations in Polymeric Microscale Mechanical Metamaterials. *Nano Lett.* **2024**, *24*, 2735.

(27) Blankenship, B. W.; Meier, T.; Arvin, S. L.; Li, J.; Seymour, N.; De La Torre, N.; Hsu, B.; Zhao, N.; Mavrikos, S.; Li, R.; et al. Nondestructive Imaging of Manufacturing Defects in Microarchitected Materials. *ACS Appl. Eng. Mater.* **2024**, *2* (7), 1737−1742.

(28) Ladika, D.; Noirbent, G.; Dumur, F.; Gigmes, D.; Mourka, A.; Barmparis, G. D.; Farsari, M.; Gray, D. Synthesis and Application of Triphenylamine-Based Aldehydes as Photo-Initiators for Multi-Photon Lithography. *Appl. Phys. A: Mater. Sci. Process* **2022**, *128* (9), 745.

(29) Sharaf, A.; Frimat, J. P.; Kremers, G. J.; Accardo, A. Suppression of Auto-Fluorescence from High-Resolution 3D Polymeric Architectures Fabricated via Two-Photon Polymerization for Cell Biology Applications. *Micro. Nano Engineer.* **2023**, *19*, 100188.

(30) Denk, W.; Strickler, J. H.; Webb, W. W. Two-Photon Laser Scanning Fluorescence Microscopy. *Science* **1990**, *248* (4951), 73−76.

(31) Bohren, C. F.; Huffman, D. R.; Absorption and Scattering by an Arbitrary Particle. In *Absorption and Scattering of Light by Small Particles*, John Wiley & Sons, Ltd: 1998; pp. 57−81.

(32) Wriedt, T.; Mie Theory: A Review. In *The Mie Theory: basics and Applications*, Springer: Berlin, Heidelberg, 2012; pp. 53−71. .

(33) Cheng, L.-C.; Horton, N. G.; Wang, K.; Chen, S.-J.; Xu, C. Measurements of Multiphoton Action Cross Sections for Multiphoton Microscopy. *Biomed. Opt. Express* **2014**, *5* (10), 3427−3433.

(34) Barad, Y.; Eisenberg, H.; Horowitz, M.; Silberberg, Y. Nonlinear Scanning Laser Microscopy by Third Harmonic Generation. *Appl. Phys. Lett.* **1997**, *70* (8), 922−924.

(35) Müller; Squier; Brakenhoff. 3D Microscopy of Transparent Objects Using Third-Harmonic Generation. *J. Microsc.* **1998**, *191* (3), 266−274.

(36) Squier, J. A.; Müller, M.; Brakenhoff, G. J.; Wilson, K. R. Third Harmonic Generation Microscopy. *Opt. Express* **1998**, *3* (9), 315−324.

(37) Luo, H.-C.; Zhao, Y.-Y.; Zhao, X.-Y.; Cao, Y.-Y.; Duan, X.-M. Grayscale Two-Photon 3D Printed Gradient-Refractive-Index Metamaterial Lens for Dual-Band Mid-Infrared Imaging. *APL Photonics* **2024**, *9* (5), 051303.

(38) Wang, H.; Pan, C.-F.; Li, C.; Menghrajani, K. S.; Schmidt, M. A.; Li, A.; Fan, F.; Zhou, Y.; Zhang, W.; Wang, H.; et al. Two-Photon Polymerization Lithography for Imaging Optics. *Int. J. Extrem. Manuf.* **2024**, *6* (4), 042002.

(39) Littlefield, A. J.; Xie, D.; Richards, C. A.; Ocier, C. R.; Gao, H.; Messinger, J. F.; Ju, L.; Gao, J.; Edwards, L.; Braun, P. V.; et al. Enabling High Precision Gradient Index Control in Subsurface Multiphoton Lithography. *ACS Photonics* **2023**, *10* (9), 3008−3019.

(40) Flamourakis, G.; Kordas, A.; Barmparis, G. D.; Ranella, A.; Farsari, M. Low-Autofluorescence Transparent Composite for Multiphoton 3D Printing. *Opt. Mater. Express* **2021**, *11* (3), 801−813.

(41) Kunwar, P.; Toivonen, J.; Kauranen, M.; Bautista, G. Third-Harmonic Generation Imaging of Three-Dimensional Microstructures Fabricated by Photopolymerization. *Opt. Express* **2016**, *24* (9), 9353−9358.

(42) Kallioniemi, L.; Annurakshita, S.; Bautista, G. Third-Harmonic Generation Microscopy of Undeveloped Photopolymerized Structures. *OSA Continuum, OSAC* **2020**, *3* (11), 2961−2967.

(43) Vangelatos, Z.; Sheikh, H. M.; Marcus, P. S.; Grigoropoulos, C. P.; Lopez, V. Z.; Flamourakis, G.; Farsari, M. Strength through Defects: A Novel Bayesian Approach for the Optimization of Architected Materials. *Sci. Adv.* **2021**, *7* (41), No. eabk2218.

(44) Vangelatos, Z.; Komvopoulos, K.; Grigoropoulos, C. Vacancies for Controlling the Behavior of Microstructured Three-Dimensional Mechanical Metamaterials. *Math. Mech. Solids* **2019**, *24* (2), 511−524.

(45) Ladika, D.; Butkus, A.; Melissinaki, V.; Skliutas, E.; Kabouraki, E.; Juodkazis, S.; Farsari, M.; Malinauskas, M. X-Photon 3D Lithography by Fs-Oscillators: Wavelength-Independent and Photo-initiator-Free. *Gxjzz* **2024**, *5*, 1.

(46) Kotz, F.; Quick, A. S.; Risch, P.; Martin, T.; Hoose, T.; Thiel, M.; Helmer, D.; Rapp, B. E. Two-Photon Polymerization of Nanocomposites for the Fabrication of Transparent Fused Silica Glass Microstructures. *Adv. Mater.* **2021**, *33* (9), 2006341.

(47) Li, F.; Liu, S.-F.; Liu, W.; Hou, Z.-W.; Jiang, J.; Fu, Z.; Wang, S.; Si, Y.; Lu, S.; Zhou, H.; et al. 3D Printing of Inorgani Nanomaterials by Photochemically Bonding Colloidal Nanocrystals. *Science* **2023**, *381* (6665), 1468−1474.

(48) Wu, J.; Liang, Y.; Chen, S.; Hsu, C.-L.; Chavarha, M.; Evans, S. W.; Shi, D.; Lin, M. Z.; Tsia, K. K.; Ji, N. Kilohertz Two-Photon Fluorescence Microscopy Imaging of Neural Activity in Vivo. *Nat. Methods* **2020**, *17* (3), 287−290.

(49) Ovsianikov, A.; Viertl, J.; Chichkov, B.; Oubaha, M.; MacCraith, B.; Sakellari, I.; Giakoumaki, A.; Gray, D.; Vamvakaki, M.; Farsari, M.; et al. Ultra-Low Shrinkage Hybrid Photosensitive Material for Two-Photon Polymerization Microfabrication. *ACS Nano* **2008**, *2* (11), 2257−2262.

(50) Zyla, G.; Maconi, G.; Nolvi, A.; Marx, J.; Ladika, D.; Salmi, A.; Melissinaki, V.; Kassamakov, I.; Farsari, M. 3D Micro-Devices for Enhancing the Lateral Resolution in Optical Microscopy. *Gxjzz* **2024**, *5*, 1−14.

(51) Pan, D.; Rivera, J. A.; Kim, P.; Miao, M.; Tyml, T.; Rodríguez, C.; Wang, B.; Yoshikuni, Y.; Elisabeth, N. H.; Northen, T.; et al. Label-Free Structural Imaging of Plant Roots and Microbes Using Third-Harmonic Generation Microscopy. *bioRxiv* **2024**, 589377.

(52) Akturk, S.; Gu, X.; Kimmel, M.; Trebino, R. Extremely Simple Single-Prism Ultrashort- Pulse Compressor. *Opt. Express* **2006**, *14* (21), 10101−10108.